

# Tuning Charge Carrier and Spin Transport Properties via Structural Modification of Polymer Semiconductors

Dong Li,<sup>†,§</sup> Xiang Wang,<sup>‡,§,||</sup> Zuzhang Lin,<sup>†</sup> Yuanhui Zheng,<sup>†</sup> Qianqing Jiang,<sup>†</sup> Naihang Zheng,<sup>†,§</sup> Weifeng Zhang,<sup>†</sup> Kui-juan Jin,<sup>\*,‡,§,||</sup> and Gui Yu<sup>\*,†,§</sup>

<sup>†</sup>Beijing National Laboratory for Molecular Sciences, CAS Research/Education Center for Excellence in Molecular Sciences, Institute of Chemistry, Chinese Academy of Sciences, Beijing 100190, P. R. China

<sup>‡</sup>Beijing National Laboratory for Condensed Matter Physics, Institute of Physics, Chinese Academy of Sciences, Beijing 100190, P. R. China

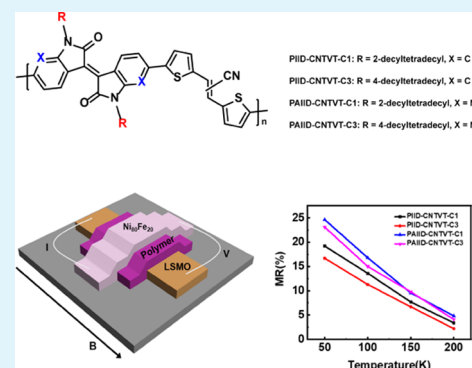
<sup>§</sup>University of Chinese Academy of Sciences, Beijing 100049, P. R. China

<sup>||</sup>Songshan Lake Materials Laboratory, Dongguan, Guangdong 523808, P. R. China

## Supporting Information

**ABSTRACT:** Targeted design of organic semiconductors in organic spintronics is relatively limited. Therefore, four conjugated polymers with analogous structures based on isoindigo (IID) units were designed and synthesized to investigate the structure–property relationships in spin and charge carrier transport. Structural design strategies include introduction of pyridinic nitrogen atoms into IID units to change electronic structures and alteration of different branching points of alkyl chains to adjust the aggregation structure. By fabricating polymer field-effect transistors (PFETs) and organic spin valves (OSVs), all of the polymers exhibited good ambipolar field-effect properties (all of the mobilities exceeding  $0.3 \text{ cm}^2 \text{ V}^{-1} \text{ s}^{-1}$ ) and relatively high magnetoresistance (MR) values (maximum up to 25%). Most importantly, it is found that the introduction of pyridinic nitrogen into the IID units can improve MR values of OSVs and electron mobilities of PFETs, whereas the extension of alkyl chain branching points can reduce MR values of the conjugated polymers. This work is the first attempt to thoroughly study the structure–property relationship in the OSVs, combined with molecular design of the conjugated polymers, which provides a guideline for molecular engineering, especially for organic spintronics.

**KEYWORDS:** polymer semiconductors, organic spin valves, molecular design, field-effect transistors, mobility



## INTRODUCTION

Spintronics is a rising interdisciplinary to study the degree of freedom of electronic spin to realize efficient data operations and information storage.<sup>1</sup> Over recent years, organic semiconductors (OSCs) for use in spintronics have attracted the attention from the materials community,<sup>2</sup> the so-called organic spintronics.<sup>3</sup> These materials, with the superiorities including structure tunability, easy processability, and low cost,<sup>4</sup> as well as inherently weak spin orbital coupling and hyperfine interaction,<sup>5,6</sup> are unexceptionable candidates for new-generation spin devices.<sup>7,8</sup> As the fundamental devices in organic spintronics, organic spin valves (OSVs) are composed of an organic nonmagnetic interlayer between two different magnetic electrodes. Based on the OSV devices, different OSCs are utilized as organic nonmagnetic interlayers to study device physics and potential applications. Tris(8-hydroxyquinoline)aluminum (Alq<sub>3</sub>), the first and extensively studied OSCs,<sup>9</sup> to our knowledge, possesses the maximum magnetoresistance (MR) value up to 300%.<sup>10,11</sup> In addition to pursuing higher MR values, the hybrid organic/inorganic interfaces between OSCs and magnetic electrodes attract significant interest.<sup>12–14</sup>

Discoveries of inverse MR and interpretations of their mechanism are important components,<sup>15</sup> which are mainly attributed to the hybridization of organic/inorganic interfaces, the so-called spinterface.<sup>16,17</sup> The hybrid interfaces can be designed by introducing an interfacial layer, including polar layers,<sup>18</sup> small molecules,<sup>19</sup> self-assembled organic molecules and single-molecule magnets,<sup>20,21</sup> radicals monolayers,<sup>22</sup> and magnetic oxide layers to modify the spin injection.<sup>23</sup> On the other hand, the study on functional devices based on OSVs is also one of the most important topics, which primarily concentrates on integration with light,<sup>24</sup> electricity and magnetism adjustment on OSVs,<sup>25</sup> to achieve the purpose of particular functionalities.<sup>26</sup> As a typical case, light-emitting diodes based on spin-polarized current recently realized the magneto-electroluminescence (MEL) response of 2.4% at 9 V,<sup>27</sup> where the higher operation voltage and MEL are the two more steps for practical applications of synergy between

Received: May 5, 2019

Accepted: July 25, 2019

Published: July 25, 2019

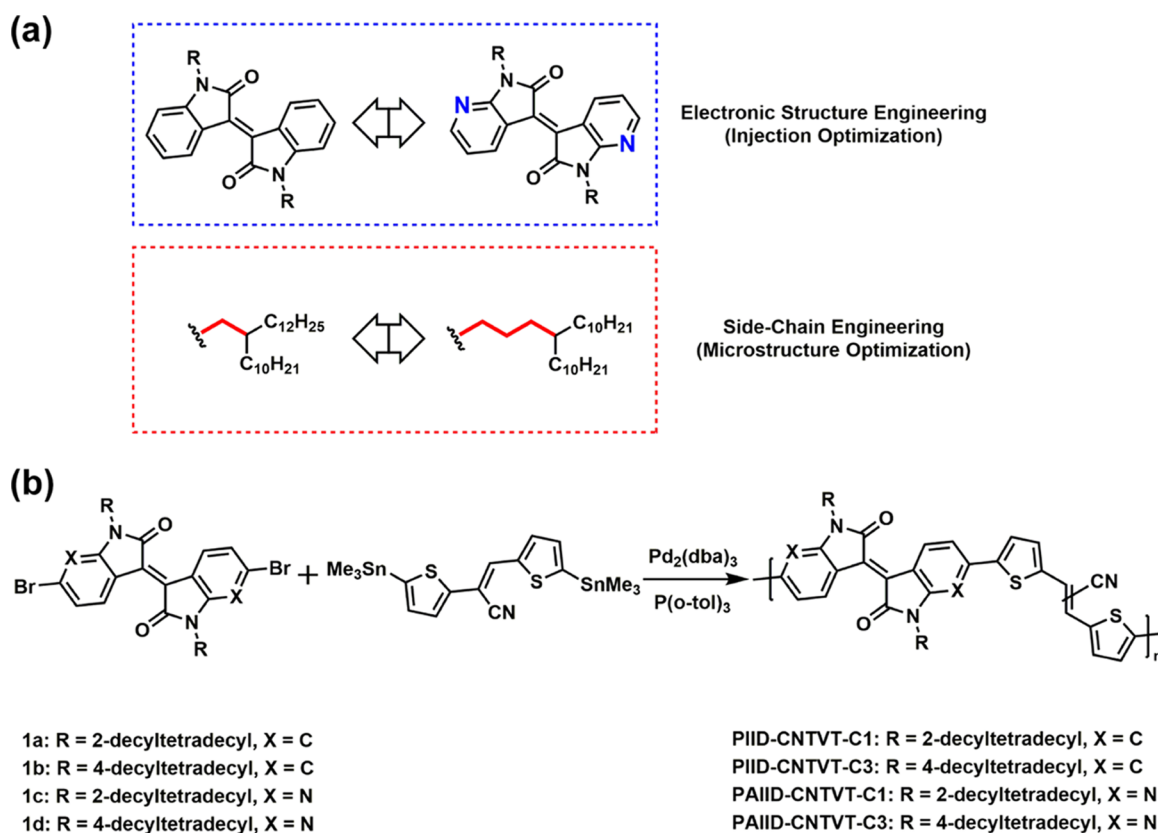


Figure 1. (a) Molecular design strategy. (b) Synthetic route of the four conjugated polymers.

magnetic field and light emission.<sup>28</sup> For another, a molecular spin-photovoltaic device was fabricated for the first time with magnetophotovoltage response of up to 5% at room temperature, in which spin-polarized currents could be generated by photogenerated carriers.<sup>24</sup>

Among all of the highlighted works, the OSCs are always the protagonists in the field of organic spintronics, from initially small molecules including  $\text{Alq}_3$ ,<sup>9</sup>  $\text{F}_{16}\text{CuPc}$ ,<sup>29</sup> rubrene,<sup>30,31</sup> and fullerene<sup>32,33</sup> to polymers containing P3HT,<sup>34</sup> P(NDI2OD-T2),<sup>35</sup> and DOO-PPV.<sup>5</sup> To some extent, different molecular structures put an important effect on the performance of OSVs,<sup>36</sup> where subtle variations can influence spin transport properties, especially for polymers.<sup>5</sup> However, chemical superiorities are yet to be realized that targeted design and synthesis of organic spintronics are underdeveloped. Besides, the relevant relationships between molecular structures of the organic interlayers and the performances of OSVs are overlooked among previous reports. Moreover, all of the OSCs reported in this field are commercially available and there are a few materials designed, especially for organic spintronics study.

Therefore, we designed four structural analogues of isoidindigo (IID)-based donor–acceptor (D–A) copolymers with the introduction of pyridinic nitrogen into the IID units and alkyl chains with different branching points to study the correlation of polymer structures with their spin and charge carrier transport properties. The envisioned principles for molecular design are mainly the features of D–A type polymers that shine in the field of organic electronics and generally exhibit high charge carrier mobilities because of lower-energy charge transfer transition from electron density gradient along the conjugated skeleton with the optimized

highest occupied molecular orbital (HOMO) and lowest unoccupied molecular orbital (LUMO),<sup>37,38</sup> where high charge carrier mobility is conducive to spin relaxation and thus outstanding spin transport.<sup>39</sup> With the obtained four polymers, we figure out the variation of electronic structures and energy levels by characterization of the optical and electrochemical properties, as well as the effect of structural modification by microstructures and morphologies of thin films. Furthermore, by fabricating spin valves and field-effect transistors based on the four conjugated polymers, we demonstrated that introduction of the pyridinic nitrogen into IID affords a higher magnetoresistance and electron mobility. This enhancement may be from the reduced polymeric LUMO energy levels, leading to ready injection of both the spin-polarized and equilibrated electrons. Different side-chain motifs also affect the microstructures of thin films and thus the charge carrier and spin transport properties. Such molecular design strategies should be used in polymer field-effect transistors (PFETs), but infrequently in OSVs, which is propitious to the widespread application of OSVs and to expand the scope of this field from device physics to materials science.

## EXPERIMENTAL SECTION

**Instruments and Measurement.** All starting chemicals were commercially available and utilized directly. The monomers were synthesized according to previous reports. A Bruker DMX 300 spectrometer was used to record  $^1\text{H}$  NMR spectra of all molecules with the internal standard tetramethylsilane. UV–vis–NIR absorption spectra were obtained by a Hitachi J-570 spectrophotometer. The molecular weights were measured by gel permeation chromatography with a PL-220 system at 150 °C, where 1,2,4-trichlorobenzene was adopted as an eluent. The polymeric films surface morphologies were clarified by a Digital Instruments Nanoscope V atomic force

microscope (AFM) with tapping mode. The PFETs and electronic properties of the spin valve devices were measured by a Keithley 4200 semiconductor characterization system. Magnetic and cryogenic correlated tests of the spin valve devices were characterized by a Quantum Design physical property measurement system (PPMS).

**General Procedures for Stille Polymerization.** All of the monomers were synthesized in accordance with the earlier literature works.<sup>40–42</sup> As shown in Figure 1b, the two kinds of monomers, (*E*)-2,3-bis(5′-(trimethylstannyl)thiophen-2′-yl)acrylonitrile (0.20 mmol) and dibromo-IID (0.20 mmol) or dibromo-AIID (0.20 mmol), were added to a 50 mL Schlenk flask and Pd<sub>2</sub>(dba)<sub>3</sub> (9.0 mg), P(*o*-tol)<sub>3</sub> (24.6 mg), and chlorobenzene (8 mL) were added in order. The flask was charged with argon when the freeze–pump–thaw cycle was carried out three times, and at 120 °C, the agitating process was carried out for 20 h. Then, the resulting mixture was added with 200 mL of methanol before filtration. Next, to further purify the leached residue, Soxhlet extraction was carried out in sequence with methanol, acetone, as well as hexane. At last, the final polymer was obtained by chloroform extraction.

**PIID-CNTVT-C1** (191.6 mg, 83%). GPC:  $M_n = 16.1$  kDa, PDI = 2.12. <sup>1</sup>H NMR (300 MHz, CDCl<sub>3</sub>)  $\delta$ : 9.14–8.78 (br, 2H), 7.50–7.00 (br, 9H), 3.67 (s, 4H), 2.02 (m, 2H), 1.46–1.16 (m, 80H), 0.97–0.88 (m, 12H). Elemental Anal. Calcd for C<sub>75</sub>H<sub>109</sub>N<sub>3</sub>O<sub>2</sub>S<sub>2</sub>: C 78.41, H 9.56, N 3.66. Found: C 78.05, H 9.48, N 3.64.

**PIID-CNTVT-C3** (167.7 mg, 73%). GPC:  $M_n = 21.3$  kDa, PDI = 2.35. <sup>1</sup>H NMR (300 MHz, CDCl<sub>3</sub>)  $\delta$ : 9.20–8.83 (br, 2H), 7.50–7.00 (br, 9H), 3.84 (m, 4H), 2.06 (m, 4H), 1.55–1.25 (m, 78H), 0.97–0.88 (m, 12H). Elemental Anal. Calcd for C<sub>75</sub>H<sub>109</sub>N<sub>3</sub>O<sub>2</sub>S<sub>2</sub>: C 78.41, H 9.56, N 3.66. Found: C 77.98, H 9.49, N 3.63.

**PAIID-CNTVT-C1** (197.9 mg, 86%). GPC:  $M_n = 18.0$  kDa, PDI = 1.95. <sup>1</sup>H NMR (300 MHz, CDCl<sub>3</sub>)  $\delta$ : 9.21 (br, 2H), 7.50–7.20 (br, 7H), 3.74 (s, 4H), 1.97 (m, 2H), 1.46–1.16 (m, 80H), 0.78 (m, 12H). Elemental Anal. Calcd for C<sub>73</sub>H<sub>107</sub>N<sub>3</sub>O<sub>2</sub>S<sub>2</sub>: C 76.19, H 9.37, N 6.09. Found: C 75.76, H 9.31, N 6.04.

**PAIID-CNTVT-C3** (186.4 mg, 81%). GPC:  $M_n = 23.8$  kDa, PDI = 2.10. <sup>1</sup>H NMR (300 MHz, CDCl<sub>3</sub>)  $\delta$ : 9.12 (br, 2H), 7.60–6.96 (br, 7H), 3.84 (m, 4H), 2.06 (m, 4H), 1.32–1.12 (m, 78H), 0.89–0.76 (m, 12H). Elemental Anal. Calcd for C<sub>73</sub>H<sub>107</sub>N<sub>3</sub>O<sub>2</sub>S<sub>2</sub>: C 76.19, H 9.37, N 6.09. Found: C 76.22, H 9.44, N 6.11.

**Details of Device Fabrication.** The polymeric field-effect transistors (PFETs) were fabricated on the Coning glass with top-gate bottom-contact configuration (TGBC). In a vacuum evaporation system, the gold source–drain electrodes were deposited via a shadow mask, with a channel width of 1400  $\mu\text{m}$  and a channel length of 50  $\mu\text{m}$ , respectively. Then, the solutions of copolymers ( $\sim 5$  mg mL<sup>-1</sup> in CHCl<sub>3</sub>) were spin-coated in a nitrogen glovebox, annealed at an appropriate temperature. Subsequently, as the dielectric layer, the solution of poly(methylmethacrylate) (PMMA) was spin-coated (about 1  $\mu\text{m}$  thick) and annealed for half an hour at 80 °C. Aluminum was then evaporated via a mask on the PMMA films as the gate electrode. The field-effect charge mobility,  $\mu$ , is obtained by the saturation regime equation  $I_{\text{DS}} = (W/2L) \times \mu \times C_i \times (V_{\text{GS}} - V_{\text{th}})^2$ , in which  $I_{\text{DS}}$  refers to the source–drain current and  $C_i$  refers to the dielectric layer's capacitance. The relative dielectric constant of dielectric layers was measured to be 2.7.  $W$  and  $L$  represent the channel width and length, respectively.  $V_{\text{GS}}$  refers to the gate voltage, and  $V_{\text{th}}$  is the threshold voltage.

As for the fabrication of spin valve devices, first, the La<sub>2/3</sub>Sr<sub>1/3</sub>MnO<sub>3</sub> (LSMO) film (about 50 nm thick) was deposited by a physical pulsed laser deposition method on SrTiO<sub>3</sub> (STO) (100) substrates and then etched to strip pattern (250  $\mu\text{m} \times 2.5$  nm) by an ion beam etching process as the bottom electrode. Next, the polymeric chloroform solutions (about 5 mg mL<sup>-1</sup>) were prepared and spin-coated on the LSMO electrodes (3000 rpm) and the films' thickness was measured to be about 40 nm. Finally, by thermal evaporation with a shadow mask, Ni<sub>80</sub>Fe<sub>20</sub> (10 nm) serving as the top electrode and Au (20 nm) as the covering layer were deposited.

## RESULTS AND DISCUSSION

**Synthesis and Thermal Properties.** Isoindigo-based copolymers have become an important class of semiconducting polymers with versatility,<sup>43,44</sup> which especially possess high change carrier mobilities in polymeric field-effect transistors (PFETs) that may favor potentially long spin relaxation length. Therefore, we chose this type of polymers to study their potential spin transport features. The moderate electron-deficiency of isoindigo derivative ensures the low-lying energy levels of hybridized molecular orbitals. To disclose the effect of electronic structures, we introduced additional pyridinic nitrogen atoms into the isoindigo skeleton to further enhance the electron-accepting behavior and planarize the polymer backbone when coupled with thiophene-derivative subunits. The other building unit is dithienylacrylonitrile (CNTVT). This building block can dramatically inverse the charge polarity from hole to electron transport due to the nitrile substitution. Both building blocks can realize the electronic structure engineering and optimize charge carrier and spin transport properties. To modulate the microstructural parameters of the polymer thin films, we introduced two different alkyl side chains, 2-decyltetradecyl (C1) and 4-decyltetradecyl (C3) groups, into polymer backbones, in which branching points are altered to tune the intermolecular interactions of polymer aggregates, and thus to influence the properties of interface and surface in electronic devices. In short, the molecular structures, microstructures of the films, and transport properties of both charge carriers and spin-polarized currents are tuned by two structural parameters of the side-chain branching point and the embedded pyridinic nitrogen atoms, as concluded in Figure 1a. The synthetic routes of the four polymers, PIID-CNTVT-C1, PIID-CNTVT-C3, PAIID-CNTVT-C1, and PAIID-CNTVT-C3, are shown in Figure 1b. The ready access to polymers involves the use of standard Stille reaction between a series of monomers 1 (a–d) and ditiin monomers in the presence of Pd catalysts. All of the four polymers with moderate molecular weights were obtained in good yields.

To study polymeric thermal properties, thermal gravimetric analysis was carried out. As shown in Figure S1, the percentages by weight of different polymers decreases as the temperature increases. We define  $T_{\text{dec}}$  as the temperature of 5% loss of polymeric weight.  $T_{\text{dec}}$  of PIID-CNTVT-C3 is 389 °C, while the one of PAIID-CNTVT-C3 increases to 399 °C. When the branching points of alkyl chains are closer to conjugated skeleton, significant reductions of  $T_{\text{dec}}$  to 386 and 375 °C separately correspond to PIID-CNTVT-C1 and PAIID-CNTVT-C1. The results demonstrate that all the polymers hold a good thermal stability.

**Optical and Electrochemical Properties.** To figure out polymeric optical properties, as illustrated in Figure 2, UV–visible–near infrared (NIR) absorption spectra were measured under the chloroform solution and thin film. All of the polymers have the similar dual-band absorption profiles, consisting of the narrow bands in the range of 300–500 nm, as well as the board ones of 500–800 nm. In general, the low-energy absorption of long-wave band is mainly due to the intramolecular charge transfers from donor to acceptor moieties. Absorption maxima ( $\lambda_{\text{max}}^{\text{abs}}$ ) of both PIID-CNTVT-C1 and PIID-CNTVT-C3 in chloroform are approximately 700 and 698 nm, whereas those of PAIID-CNTVT-C1 and PAIID-CNTVT-C3 are red-shifted to 702 and 720 nm, respectively. This phenomenon is likely attributed to the

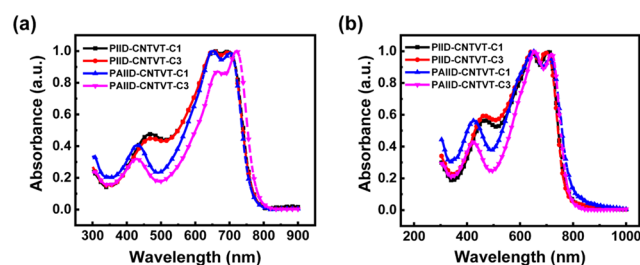


**Figure 2.** Normalized UV-vis-NIR absorption spectra of the four conjugated copolymers in (a) chloroform and (b) thin film.

increased backbone planarization because pyridinic nitrogen can readily reduce the interunit steric hindrance.

Moreover, the corresponding absorption spectra in thin films are broadened because of enhanced molecular aggregations, compared with those in solution. Interestingly, the absorption profiles of both PIID-CNTVT-C1 and PAIID-CNTVT-C1 thin films, featuring identical branching points, are red-shifted to 707 and 713 nm, respectively, compared with those in the solutions. The absorption maxima of other two polymers with 4-decyltetradecyl side chains, PIID-CNTVT-C3 and PAIID-CNTVT-C3, are slightly blue-shifted to 696 and 718 nm, respectively. This result is mainly due to the different vibronic structures originating from branching points that can influence the molecular aggregation in thin film. The optical gaps were calculated by using thin-film absorption onset, as shown in Table 1. The AIID-based polymers exhibit narrower optical gaps because the planarization of polymer backbone enhances  $\pi$ -delocalization.

To obtain the estimated frontier orbital energy levels, cyclic voltammetry (CV) analyses of the four polymeric thin films were conducted at an Ar atmosphere. The resulting data, calculated from the CV traces in Figure S2, are tabularized in Table 1. The HOMO and LUMO energy levels were obtained to be  $-5.54/-3.56$  and  $-5.62/-3.58$  eV for PIID-CNTVT-C1 and PIID-CNTVT-C3, respectively, whereas those of PAIID-CNTVT-C1 and PAIID-CNTVT-C3 are  $-5.75/-3.66$  and  $-5.77/-3.72$  eV, respectively. This result indicated that the introduction of electron-accepting pyridinic nitrogen atoms reduced the HOMO and LUMO energy levels. This reduction could affect charge carriers and spin injection from electrodes, thus possibly influencing charge carrier mobilities of PFETs and MR values of OSVs.

From Table 1, in the band gap perspective, the difference exists between band gaps from CV and optical gaps, which is mainly due to exciton binding energies.<sup>42</sup> Meanwhile, in our fabricated devices, the polymers are in the solid film form of existence. To verify the HOMO energy levels, as depicted in Figure 3, the ultraviolet photoelectron spectroscopy (UPS) measurements were performed on polymer thin films on silica substrates. The ionization potentials (IPs), estimated from the

equation  $IP = h\nu - (E_{\text{cutoff}} - E_{\text{H,onset}})$  eV, were acquired to be 5.54, 5.53, 5.76, and 5.77 eV for PIID-CNTVT-C1, PIID-CNTVT-C3, PAIID-CNTVT-C1, and PAIID-CNTVT-C3, respectively, which are consistent with the data obtained from CV analysis that the presence of pyridinic nitrogen atoms can reduce the frontier orbital energy levels.

**Polymeric Field-Effect Transistors.** To unveil the polymeric charge transport properties, we fabricated PFETs on Coning glass substrates with TGBC-configuration, where the encapsulation effect confers device stability under ambient conditions, especially for electron transport. Detailed procedures of devices fabrications and measurements are given in the Experimental Section. The PFETs exhibit representative transfer and output curves, as depicted in Figures 4 and S2. Obviously, all of the polymers present excellent ambipolar charge transport behaviors. As summarized in Table 2, the calculated maximum electron/hole mobilities of PIID-CNTVT-C1 and PIID-CNTVT-C3 based devices are 0.63/1.22 and 0.36/0.67  $\text{cm}^2 \text{V}^{-1} \text{s}^{-1}$ , respectively. When the pyridinic nitrogen atoms are introduced into the conjugate skeleton, the devices reveal higher electron and lower hole mobilities of 3.10/0.30 and 1.01/0.40  $\text{cm}^2 \text{V}^{-1} \text{s}^{-1}$  for PAIID-CNTVT-C1 and PAIID-CNTVT-C3, respectively.

The above results show that the introduction of nitrogen atoms reduced the hole mobilities and improved the electron mobilities, whereas extension of the methylene spacers between the backbone and the branching point of the alkyl chain reduced the electron/hole mobilities, except for the hole mobility of PAIID-CNTVT-C3. Combined with energy levels of polymers measured above, we suppose that higher HOMO energy levels are one of the reasons for higher hole mobilities of two polymers based on the IID units, which are partly conducive to the hole injection from the frequently used Au electrode to polymer semiconductors. In contrast, the lower LUMO energy levels of PAIID-CNTVT-C1 and PAIID-CNTVT-C3 improved their electron mobilities, to a certain extent. Therefore, these results indicated a clear structure-property relationship that the energy levels determined by molecular structure extremely influence the electron/hole mobilities of polymers. Moreover, PAIID-CNTVT-C3, compared with the nitrile-absent polymer PAIID-DTE-C3, was characterized with higher electron and lower hole mobilities because introduction of an electron-withdrawing nitrile group to a molecular backbone remarkably improved the efficient electron injection.<sup>45</sup>

**Polymeric Spin Valves.** Our synthesized polymers possess excellent charge transport properties, which is beneficial to spin relaxation.<sup>38</sup> To examine spin transport in the polymers, we fabricated OSVs combining two different ferromagnetic electrodes and a switched polymer interlayer. Different relative magnetization alignments of ferromagnetic electrodes under the varying magnetic field determine whether spin-polarized

**Table 1.** Optical and Electrochemical Properties of the Four Conjugated Polymers

polymers	$\lambda_{\text{max}}^{\text{abs}}$ (nm)	$E_{\text{g}}^{\text{opt}}$ (eV)	HOMO (eV) <sup>a</sup>	LUMO (eV) <sup>a</sup>	ionization potentials (eV) <sup>b</sup>	electron affinity (eV) <sup>c</sup>
PIID-CNTVT-C1	656, 698 <sup>d</sup> /646, 708 <sup>e</sup>	1.57	-5.54	-3.56	5.54	3.97
PIID-CNTVT-C3	654, 698 <sup>d</sup> /646, 696 <sup>e</sup>	1.58	-5.62	-3.58	5.53	3.95
PAIID-CNTVT-C1	652, 702 <sup>d</sup> /648, 714 <sup>e</sup>	1.52	-5.75	-3.66	5.76	4.24
PAIID-CNTVT-C3	666, 722 <sup>d</sup> /656, 718 <sup>e</sup>	1.55	-5.77	-3.72	5.77	4.22

<sup>a</sup>Calculated by CV with  $E_{\text{HOMO}} = -(4.40 + E_{\text{onset}}^{\text{ox}})$  eV and  $E_{\text{LUMO}} = -(4.40 + E_{\text{onset}}^{\text{red}})$  eV. <sup>b</sup>Measured by ultraviolet photoelectron spectroscopy (UPS). <sup>c</sup>Calculated by  $E_{\text{g}}^{\text{opt}}$  and ionization potentials. <sup>d</sup>In chloroform solution. <sup>e</sup>In the thin film.

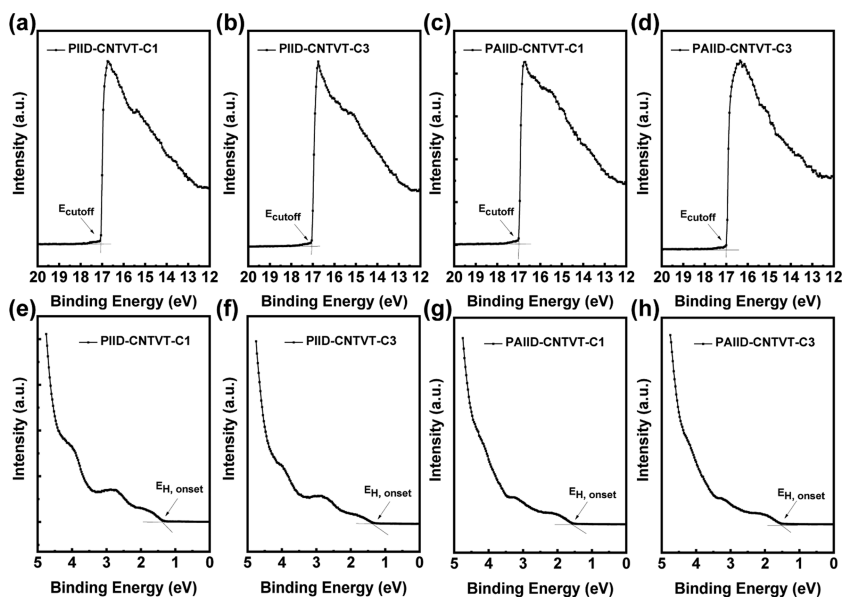


**Figure 3.** UPS spectra of (a, e) PIID-CNTVT-C1, (b, f) PIID-CNTVT-C3, (c, g) PAIID-CNTVT-C1 and (d, h) PAIID-CNTVT-C3 thin films ( $h\nu = 21.22$  eV).

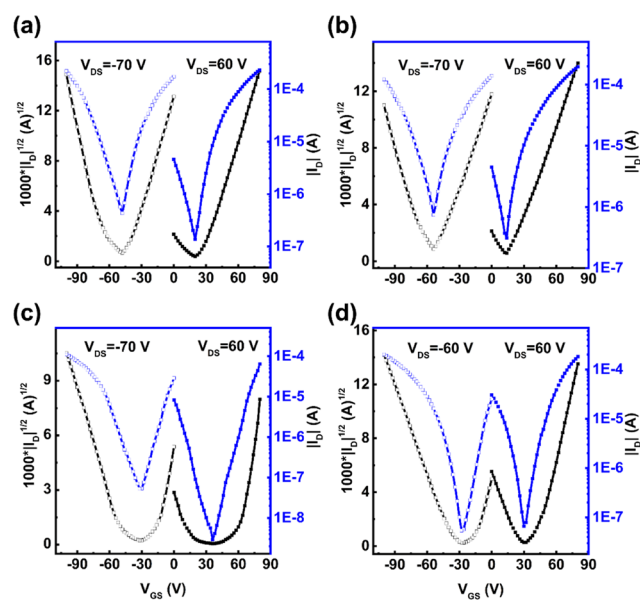


**Figure 4.** Transfer characteristics of the PFET based on (a) PIID-CNTVT-C1, (b) PIID-CNTVT-C3, (c) PAIID-CNTVT-C1, and (d) PAIID-CNTVT-C3.

current can smoothly propagate across the polymer interlayer. The device properties were estimated by MR values, which is

defined as  $MR = (R_{ap} - R_p)/R_p$ , where  $R_{ap}$  and  $R_p$  denote the resistance in the antiparallel and parallel states of ferromagnetic electrode magnetization direction, respectively. Lanthanum strontium manganite (LSMO), a half-metallic ferrimagnet with a nearly 100% spin polarization and atmospheric stability,<sup>9</sup> was selected as the bottom electrodes. Next, the polymers were spin-coated onto the LSMO bottom electrodes and top  $Ni_{80}Fe_{20}$  electrodes were evaporated on the polymeric thin films by vacuum thermal evaporation. As depicted in the inset of Figure 5a, the ultimate device structures present LSMO/polymer/ $Ni_{80}Fe_{20}$  and the junction areas were  $0.25 \times 0.36$  mm<sup>2</sup>. Energy-level diagram for the LSMO/polymer/ $Ni_{80}Fe_{20}$  stacks of spin valve devices is listed in Figure 5b.

To figure out the charge/spin transport mechanism of the OSVs, the electrical measurements were performed, as described in Figures 6 and S3. All of the  $I-V$  curves exhibited the nonlinear feature notably, which indicates that the devices are non-Ohmic contact. We consider the charge/spin transport mechanism as carriers hopping processes because the thickness of polymer films is measured to be about 40 nm, which is much thicker than the thickness of the tunneling region ( $<15$  nm).<sup>46</sup> Otherwise, to further study the charge/spin transport mechanism, the differential conductance traces from  $I-V$  characteristics are shown in Figure S4, where the zero bias abnormal was clearly absent despite of the low signal-to-noise ratio. It demonstrates that there is no metal filament or

**Table 2.** Parameters for Microstructures and Device Performance of PFETs Based on the Four Conjugated Polymers<sup>a</sup>

polymers	<i>n</i> -channel				<i>p</i> -channel				<i>d</i> - <i>d</i> (Å)	$\pi$ - $\pi$ (Å)
	$\mu_{max}^b$	$\mu_{ave}^c$	$V_{th}$ (V)	$I_{on}/I_{off}$	$\mu_{max}$	$\mu_{ave}$	$V_{th}$ (V)	$I_{on}/I_{off}$		
PIID-CNTVT-C1	0.63	0.59	35 ( $\pm 5$ )	$10^2-10^3$	1.22	1.14	-57 ( $\pm 4$ )	$10^2-10^3$	22.63	3.56
PIID-CNTVT-C3	0.36	0.32	32 ( $\pm 5$ )	$10^2-10^3$	0.67	0.52	-55 ( $\pm 5$ )	$10^2-10^3$	23.97	3.51
PAIID-CNTVT-C1	3.01	1.74	53 ( $\pm 7$ )	$10^4$	0.30	0.22	-50 ( $\pm 5$ )	$10^3$	22.36	3.63
PAIID-CNTVT-C3	1.01	0.91	38 ( $\pm 5$ )	$10^3-10^4$	0.40	0.36	-46 ( $\pm 5$ )	$10^3-10^4$	23.58	3.51

<sup>a</sup>Mobilities were extracted from the saturation regime.  $\mu_{max}$  and  $\mu_{ave}$  are maximum and average mobilities, respectively.  $V_{th}$  is the threshold voltage.  $I_{on}/I_{off}$  is the on/off current ratio of devices. <sup>b</sup>The units of mobilities mentioned below are cm<sup>2</sup> V<sup>-1</sup> s<sup>-1</sup>. <sup>c</sup>The average mobilities were calculated from more than 10 devices.

magnetic inclusion in the polymer films.<sup>47</sup> Otherwise, the temperature dependence of OSVs' resistance ( $R-T$ ) is depicted in Figure S5a. The device resistance, about hundreds of thousand Ohm, is pretty large, which is far above the resistance of tunneling transport devices. Meanwhile, the  $R-T$  curves are monotonically increased as the temperature decreases, which is the characteristic of carrier hopping transport.<sup>29</sup> Otherwise, to further eliminate the contribution of the electrode to MR, we fabricated the LSMO/NiFe device with the same process and the results make it clear that the LSMO and NiFe electrodes present no magnetoresistance signals, as depicted in Figure S5b.

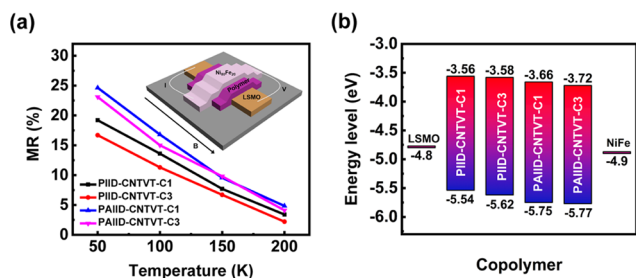


**Figure 5.** (a) Maximum MR values of OSVs at different temperatures. The inset exhibits the OSVs structure. (b) Energy-level diagram for the LSMO/polymer/ $\text{Ni}_{80}\text{Fe}_{20}$  stack.

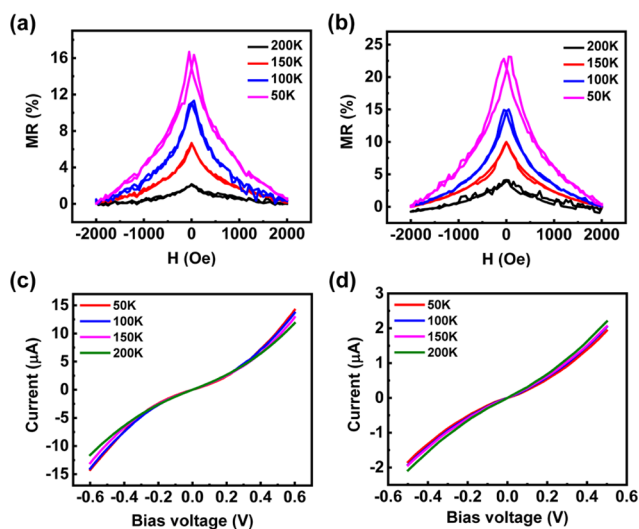


**Figure 6.** MR curves (current mode at  $0.01 \mu\text{A}$ ) and  $I-V$  curves of the OSV devices based on (a, c) PIID-CNTVT-C3 and (b, d) PAIID-CNTVT-C3 at different temperatures.

All of the polymeric spin valve devices were measured by PPMS with the pseudo-four-probe method, with the MR curves present in Figures 6 and S3. The MR traces all exhibit typical positive signals. However, the curves present the different characteristic that is without sharp switch points from the magnetic electrodes when the magnetic field scans from 2000 to  $-2000$  Oe. To clarify the inner causes, we measured the magnetic hysteresis loops of LSMO and NiFe at 100 K by a vibrating sample magnetometer in PPMS. The results are shown in Figure 7a, which traces out the great distinction of moments between LSMO and NiFe, while the NiFe possesses a pretty small coercive field. Therefore, we speculated that unsharp switch points might be from the weak magnetization of NiFe electrodes. Subsequently, we deposited NiFe on the

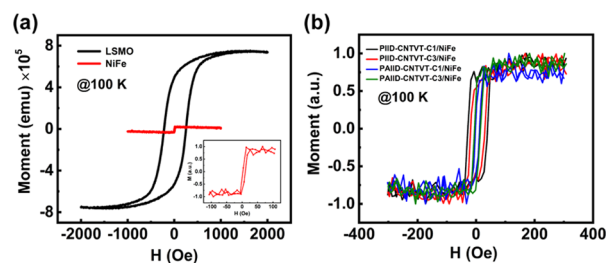


**Figure 7.** (a) Magnetic hysteresis loops of LSMO and NiFe at 100 K. The inset is the normalized ones of NiFe. (b) Magnetic hysteresis loops of NiFe with the different underlying polymers at 100 K.

different polymer films with mask and measured the magnetic hysteresis loops of NiFe electrodes on the polymer films at 100 K, as depicted with normalization in Figure 7b. It indicates that the NiFe electrodes on the polymer films exhibit different coercive fields and the coercive fields of NiFe electrodes on PIID-CNTVT-C1, PIID-CNTVT-C3, PAIID-CNTVT-C3, and PAIID-CNTVT-C1 change from the largest to smallest, which is coincident with the switch point variation trend of MR traces.

Not only MR traces exhibit certain regularity but also MR values of OSVs with different polymers present particular changes. The device based on PIID-CNTVT-C1 exhibits an MR value of 19.2% at 50 K. When the pyridinic nitrogen is introduced to the conjugated skeleton, the MR value of PAIID-CNTVT-C1 increases to 24.6% at 50 K, which is the highest among the four polymers at the same temperature. The alteration of MR values between PIID-CNTVT-C1 and PAIID-CNTVT-C1 verifies the effect of pyridinic nitrogen introduction to the conjugated skeleton. This effect can be found from the point of energy level, where lower LUMO energy levels contribute to the effective injection of spin-polarized current. The experimental phenomenon perhaps indicates that electrons dominate spin transport. Similarly, from PIID-CNTVT-C3 to PAIID-CNTVT-C3, the MR values increase from 16.7 to 23.1% at 50 K, which to a certain degree proves the speculation above. Moreover, the influences to MR values originate not only from the modification of conjugated skeletons but also from the installation of different alkyl chains. Extension of the methylene spacer to change the position of branching points from PIID-CNTVT-C1 to PIID-CNTVT-C3 brings the MR value down to 16.7% at 50 K. The variation from PAIID-CNTVT-C1 to PAIID-CNTVT-C3, analogously, makes the MR values change from 24.6 to 23.1% at 50 K. This situation may be attributed to different alkyl chains varying the microstructures of films. Meanwhile, to be expected, the attenuation of the MR signals is observed as the temperature increases. This feature originates mainly from the declined spin polarization of the LSMO electrode and enhanced spin scattering in the polymer spacers. Subsequently, as shown in Figure 5a, maximum MR values of polymeric spin valves are summarized at different temperatures. Obviously, different polymers correspond to different trends, revealing the structure–property relationship, to a certain extent. Combined with the molecular structures, for the conjugated backbones, the introduction of pyridinic nitrogen to the IID unit effectively reduces the LUMO and HOMO energy levels, according to Table 1 and Figure 5b, which is favorable for the spin-polarized current injection to the polymer to attain a higher MR value. On the other hand, variation of branching point brings about slight changes of MR values within the same

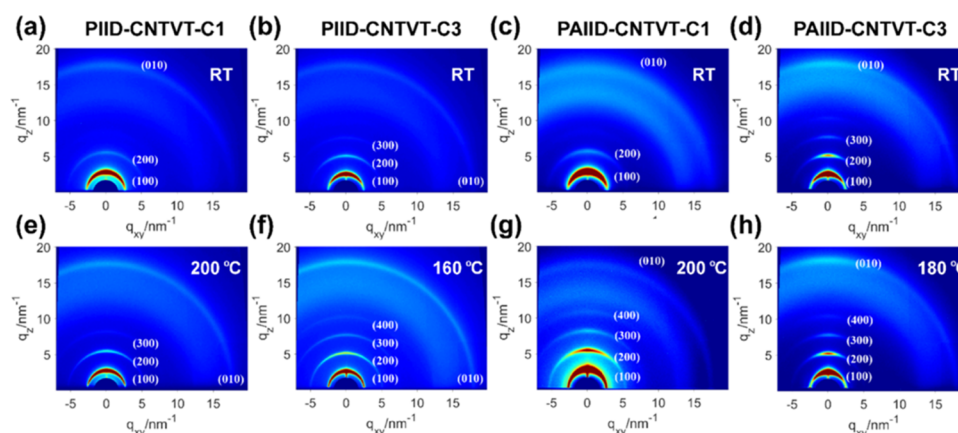


**Figure 8.** 2D-GIXRD images of the conjugated polymers before and after annealing. (a, e) PIID-CNTVT-C1, (b, f) PIID-CNTVT-C3, (c, g) PAIID-CNTVT-C1, and (d, h) PAIID-CNTVT-C3.

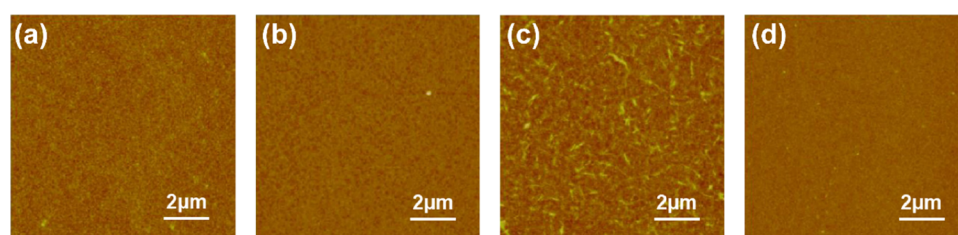


**Figure 9.** AFM images of (a) PIID-CNTVT-C1, (b) PIID-CNTVT-C3, (c) PAIID-CNTVT-C1, and (d) PAIID-CNTVT-C3 thin films after annealing.

conjugated skeleton. Especially, a higher MR value is observed when the branching point is closer to the conjugated skeleton. When the results of spin transport are compared with those of charge transport, among the four polymers, variation trend of MR values and electron charge mobilities is quite concordant.

**Microstructures and Morphologies of Films.** To further perform the structure–property relationships in both PFETs and OSVs, we investigated the film microstructures and morphologies. By the two-dimensional grazing-incidence X-ray diffraction (2D-GIXRD) technique, the thin-film microstructural information of the four polymers was investigated based on the casted and optimally annealed polymeric films on Corning glasses, as shown in Figure 8. All of the polymers present improved solid-state crystallinity and more ordered polymeric molecule packing of thin films after annealing, in out-of-plane orientations exhibiting the reinforced diffraction ( $h00$ ) peaks. The (010) peaks are present not only in the out-of-plane ( $q_z$ ) but also in the in-plane ( $q_{xy}$ ) directions for all polymers, which demonstrates that all of the four polymers adopt the mixed edge-on/face-on orientations. Meanwhile, the film of PIID-CNTVT-C1 takes on (300) diffractions peaks, whereas PIID-CNTVT-C3 and PAIID-CNTVT-C3 even present ( $h00$ ) peaks up to the fourth order, as well as PAIID-CNTVT-C1. It manifests that the annealing treatment immensely increases the crystallinity of these films.

By means of out-of-plane and in-plane directions in 2D-GIXRD diffraction patterns, the  $d$ – $d$  and  $\pi$ – $\pi$  distances were calculated by formula  $d = 2\pi/q$  according to the one-dimensional patterns of GIXRD in Figure S6 with the resulted data listed in Table 2. The values of  $d$ – $d$  distances for PIID-CNTVT-C1 and PAIID-CNTVT-C1 are 22.63 and 22.36 Å, whereas those of PIID-CNTVT-C3 and PAIID-CNTVT-C3 reach 23.97 and 23.51 Å, respectively. Obviously, the results

indicate that polymers with the same branching point possess the approximate  $d$ – $d$  distances. In fact, the distinction of  $d$ – $d$  distances among the polymers leads to the disparity of OSV MR values. More precisely, the branching points closed to the conjugated skeleton result in the shorter  $d$ – $d$  distances, accompanying with the higher corresponding MR values, which is demonstrated to be advantageous to the transport of spin-polarized current based on the properties of OSVs. This observation fully testifies that the diversity of alkyl chains directly influences microstructures of polymer films and thereby changes the charge/spin transport. Due to increased steric hindrance, the polymers with the branching point close to the conjugated skeleton possess a longer  $\pi$ – $\pi$  stacking distance. From the calculated results, the  $\pi$ – $\pi$  stacking distance is 3.56 Å for PIID-CNTVT-C1 and increases to 3.63 Å for PAIID-CNTVT-C1, whereas 3.51 and 3.54 Å correspond to PIID-CNTVT-C3 and PAIID-CNTVT-C3. Combined with the mobilities of field-effect transistors, the characteristic of polymeric  $\pi$ – $\pi$  stacking distances is seemingly in contradiction with notion that a closer  $\pi$ – $\pi$  stacking is favorable to intermolecular charge transfer and transport. Indeed, the mobilities of field-effect transistors not only are influenced by the  $\pi$ – $\pi$  stacking but also depend on the defect state density, molecular weight, etc. Thus, it needs to be further studied.

By a tapping-mode atomic force microscope (AFM), thin-film surface morphologies of the four polymers on the Corning glass substrates were investigated. The films after annealing present smooth and homogeneous surfaces, with corresponding root-mean-square (RMS) roughnesses of 0.527, 0.394, and 0.301 nm for PIID-CNTVT-C1, PIID-CNTVT-C3 and PAIID-CNTVT-C3, respectively, as exhibited in Figure 9. For the PAIID-CNTVT-C1 thin film, the profile shows the presence of fibrillar texture and the RMS roughness is 0.794

nm. All of the areas measured for calculating the roughness above are  $10 \times 10 \mu\text{m}^2$ , which demonstrates the flatness of polymeric films. For both the TGBC-configure PFETs and OSVs, relatively low roughness results in a flatter interface and the reduction of interface scattering.<sup>48,49</sup> To take both GIXRD and AFM images into account, the higher crystallinity and more ordered polymeric molecule packing of thin films of PAIID-CNTVT-C1 account for the high carrier mobility and effective spin-polarized current transport of PAIID-CNTVT-C1.

## CONCLUSIONS

We designed and synthesized four (aza)isoidigo-CNTVT polymers to explore the effects of structural modification on the performance of field-effect transistors and spin valves. All of the polymers exhibited excellent spin transport, as well as good ambipolar charge carrier transport. The introduction of pyridinic nitrogen atoms into the IID units reduces the LUMO and HOMO energy levels, which is beneficial to electron injection; thus, the highest electron mobility of more than  $3 \text{ cm}^2 \text{ V}^{-1} \text{ s}^{-1}$  is obtained by the PFET devices with PAIID-CNTVT-C1. Based on the sandwiched spin valve structure and consistent ferromagnetic electrodes, the OSV devices with PAIID-CNTVT-C1 as the polymeric spacer exhibited the highest MR value of up to approximately 25%, which is one of the highest values among polymeric spin valves with isoidigo derivatives. This result is attributable to the energy-level change owing to the introduction of pyridinic nitrogen atoms into isoidigo units. Meanwhile, compared with polymers with branching points away from conjugated skeletons, the closer ones possessed the higher MR values. This contribution is the first attempt to explore the relationship between the polymeric molecular structures of the intermediate layer and the performance of the corresponding spin valves based on isoidigo derivatives. In accordance with this strategy, the tunability of the polymeric structures realized its full potential to achieve higher performance and more multifunctional applications for organic spintronics.

## ASSOCIATED CONTENT

### Supporting Information

The Supporting Information is available free of charge on the ACS Publications website at DOI: 10.1021/acsami.9b07863.

The TGA and CV curves of the four conjugated polymers; output characteristics of polymeric OFETs; MR curves and electronic measurements of OSVs based on PIDD-CNTVT-C1 and PAIID-CNTVT-C1;  $dI/dV$  curves of OSVs; the resistance temperature curves of OSVs and resistance variation vs magnetic field of LSMO/NiFe devices; 1D patterns GIXRD of the polymer films;  $^1\text{H}$  NMR spectra of the four polymers (PDF)

## AUTHOR INFORMATION

### Corresponding Authors

\*E-mail: [kjjin@iphy.ac.cn](mailto:kjjin@iphy.ac.cn) (K.-J.J.).

\*E-mail: [yugui@iccas.ac.cn](mailto:yugui@iccas.ac.cn) (G.Y.).

### ORCID

Dong Li: 0000-0003-1213-0585

Kui-juan Jin: 0000-0002-0047-4375

Gui Yu: 0000-0001-8324-397X

## Author Contributions

The manuscript was written through contributions of all authors. All authors have given approval to the final version of the manuscript.

## Notes

The authors declare no competing financial interest.

## ACKNOWLEDGMENTS

This work was supported by the Ministry of Science and Technology of China (2017YFA0204703 and 2016YFB0401100), the National Natural Science Foundation of China (21673258, 21774134, 21474116, and 11721404), and the Chinese Academy of Sciences (XDB12030100). The GIXRD measurements were carried out at the BL14B1 Station of Shanghai Synchrotron Radiation Facility.

## REFERENCES

- (1) Žutić, I.; Fabian, J.; Sarma, S. D. Spintronics: Fundamentals and Applications. *Rev. Mod. Phys.* **2004**, *76*, 323–410.
- (2) Naber, W. J. M.; Faez, S.; van der Wiel, W. G. Organic Spintronics. *J. Phys. D: Appl. Phys.* **2007**, *40*, R205–R228.
- (3) Pramanik, S.; Stefanita, C. G.; Patibandla, S.; Bandyopadhyay, S.; Garre, K.; Harth, N.; Cahay, M. Observation of Extremely Long Spin Relaxation Times in an Organic Nanowire Spin Valve. *Nat. Nanotechnol.* **2007**, *2*, 216–219.
- (4) Wang, C.; Dong, H.; Hu, W.; Liu, Y.; Zhu, D. Semiconducting  $\pi$ -Conjugated Systems in Field-Effect Transistors: A Material Odyssey of Organic Electronics. *Chem. Rev.* **2012**, *112*, 2208–2267.
- (5) Nguyen, T. D.; Hukic-Markosian, G.; Wang, F.; Wojcik, L.; Li, X. G.; Ehrenfreund, E.; Vardeny, Z. V. Isotope Effect in Spin Response of  $\pi$ -Conjugated Polymer Films and Devices. *Nat. Mater.* **2010**, *9*, 345–352.
- (6) Geng, R.; Subedi, R. C.; Luong, H. M.; Pham, M. T.; Huang, W.; Li, X.; Hong, K.; Shao, M.; Xiao, K.; Hornak, L. A.; Nguyen, T. D. Effect of Charge Localization on the Effective Hyperfine Interaction in Organic Semiconducting Polymers. *Phys. Rev. Lett.* **2018**, *120*, No. 086602.
- (7) Sun, D.; Ehrenfreund, E.; Vardeny, Z. V. The First Decade of Organic Spintronics Research. *Chem. Commun.* **2014**, *50*, 1781–1793.
- (8) Devkota, J.; Geng, R.; Subedi, R. C.; Nguyen, T. D. Organic Spin Valves: A Review. *Adv. Funct. Mater.* **2016**, *26*, 3881–3898.
- (9) Xiong, Z. H.; Wu, D.; Vardeny, Z. V.; Shi, J. Giant Magnetoresistance in Organic Spin-Valves. *Nature* **2004**, *427*, 821–824.
- (10) Sun, D.; Yin, L.; Sun, C.; Guo, H.; Gai, Z.; Zhang, X. G.; Ward, T. Z.; Cheng, Z.; Shen, J. Giant Magnetoresistance in Organic Spin Valves. *Phys. Rev. Lett.* **2010**, *104*, No. 236602.
- (11) Barraud, C.; Seneor, P.; Mattana, R.; Fusil, S.; Bouzehouane, K.; Deranlot, C.; Graziosi, P.; Hueso, L.; Bergenti, I.; Dediu, V.; Petroff, F.; Fert, A. Unravelling the Role of the Interface for Spin Injection into Organic Semiconductors. *Nat. Phys.* **2010**, *6*, 615–620.
- (12) Cinchetti, M.; Dediu, V. A.; Hueso, L. E. Activating the Molecular Spinterface. *Nat. Mater.* **2017**, *16*, 507–515.
- (13) Jang, H.-J.; Richter, C. A. Organic Spin-Valves and Beyond: Spin Injection and Transport in Organic Semiconductors and the Effect of Interfacial Engineering. *Adv. Mater.* **2017**, *29*, No. 1602739.
- (14) Raman, K. V.; Kamerbeek, A. M.; Mukherjee, A.; Atodiresi, N.; Sen, T. K.; Lazić, P.; Caciuc, V.; Michel, R.; Stalke, D.; Mandal, S. K.; Blügel, S.; Münzenberg, M.; Moodera, J. S. Interface-Engineered Templates for Molecular Spin Memory Devices. *Nature* **2013**, *493*, 509–513.
- (15) Ding, S. S.; Tian, Y.; Li, Y.; Mi, W. B.; Dong, H. L.; Zhang, X. T.; Hu, W. P.; Zhu, D. B. Inverse Magnetoresistance in Polymer Spin Valves. *ACS Appl. Mater. Interfaces* **2017**, *9*, 15644–15651.
- (16) Ciudad, D.; Gobbi, M.; Kinane, C. J.; Eich, M.; Moodera, J. S.; Hueso, L. E. Sign Control of Magnetoresistance Through Chemically Engineered Interfaces. *Adv. Mater.* **2014**, *26*, 7561–7567.

- (17) Sanvito, S. Molecular spintronics: The Rise of Spinterface Science. *Nat. Phys.* **2010**, *6*, 562–564.
- (18) Schulz, L.; Nuccio, L.; Willis, M.; Desai, P.; Shakya, P.; Kreouzis, T.; Malik, V. K.; Bernhard, C.; Pratt, F. L.; Morley, N. A.; Suter, A.; Nieuwenhuys, G. J.; Prokscha, T.; Morenzoni, E.; Gillin, W. P.; Drew, A. J. Engineering Spin Propagation Across a Hybrid Organic/Inorganic Interface Using a Polar Layer. *Nat. Mater.* **2011**, *10*, 39–44.
- (19) Shi, S.; Sun, Z.; Bedoya-Pinto, A.; Graziosi, P.; Li, X.; Liu, X.; Hueso, L.; Dediu, V. A.; Luo, Y.; Fahlman, M. Hybrid Interface States and Spin Polarization at Ferromagnetic Metal-Organic Heterojunctions: Interface Engineering for Efficient Spin Injection in Organic Spintronics. *Adv. Funct. Mater.* **2014**, *24*, 4812–4821.
- (20) Jang, H.-J.; Lee, J.-S.; Pookpanratana, S. J.; Hacker, C. A.; Tran, I. C.; Richter, C. A. Modifying Spin Injection Characteristics in the Co/Alq<sub>3</sub> System by Using a Molecular Self-Assembled Monolayer. *J. Phys. Chem. C* **2015**, *119*, 12949–12955.
- (21) Cucinotta, G.; Poggini, L.; Pedrini, A.; Bertani, F.; Cristiani, N.; Torelli, M.; Graziosi, P.; Cimatti, I.; Cortigiani, B.; Otero, E.; Ohresser, P.; Sainctavit, P.; Dediu, A.; Dalcanale, E.; Sessoli, R.; Mannini, M. Tuning of a Vertical Spin Valve with a Monolayer of Single Molecule Magnets. *Adv. Funct. Mater.* **2017**, *27*, No. 1703600.
- (22) Brambilla, A.; Picone, A.; Giannotti, D.; Calloni, A.; Berti, G.; Bussetti, G.; Achilli, S.; Fratesi, G.; Trioni, M. I.; Vinai, G.; Torelli, P.; Panaccione, G.; Duò, L.; Finazzi, M.; Ciccacci, F. Enhanced Magnetic Hybridization of a Spinterface through Insertion of a Two-Dimensional Magnetic Oxide Layer. *Nano Lett.* **2017**, *17*, 7440–7446.
- (23) Poggini, L.; Cucinotta, G.; Pradipto, A.-M.; Scarrozza, M.; Barone, P.; Caneschi, A.; Graziosi, P.; Calbucci, M.; Cecchini, R.; Dediu, V. A.; Picozzi, S.; Mannini, M.; Sessoli, R. An Organic Spin Valve Embedding a Self-Assembled Monolayer of Organic Radicals. *Adv. Mater. Interfaces* **2016**, *3*, No. 1500855.
- (24) Sun, X.; Vélez, S.; Atxabal, A.; Bedoya-Pinto, A.; Parui, S.; Zhu, X.; Llopis, R.; Casanova, F.; Hueso, L. E. A Molecular Spin-Photovoltaic Device. *Science* **2017**, *357*, 677–680.
- (25) Liang, S.; Yang, H.; Yang, H.; Tao, B.; Djeflal, A.; Chshiev, M.; Huang, W.; Li, X.; Ferri, A.; Desfeux, R.; Mangin, S.; Lacour, D.; Hehn, M.; Copie, O.; Dumesnil, K.; Lu, Y. Ferroelectric Control of Organic/Ferromagnetic Spinterface. *Adv. Mater.* **2016**, *28*, 10204–10210.
- (26) Guo, L.; Gu, X.; Zhu, X.; Sun, X. Recent Advances in Molecular Spintronics: Multifunctional Spintronic Devices. *Adv. Mater.* **2019**, *294*, No. 1805355.
- (27) Nguyen, T. D.; Ehrenfreund, E.; Vardeny, Z. V. Spin-Polarized Light-Emitting Diode Based on an Organic Bipolar Spin Valve. *Science* **2012**, *337*, 204–209.
- (28) Prieto-Ruiz, J. P.; Miralles, S. G.; Prima-García, H.; López-Muñoz, A.; Riminucci, A.; Graziosi, P.; Aeschlimann, M.; Cinchetti, M.; Dediu, V. A.; Coronado, E. Enhancing Light Emission in Interface Engineered Spin-OLEDs through Spin-Polarized Injection at High Voltages. *Adv. Mater.* **2019**, *31*, No. 1806817.
- (29) Sun, X.; Bedoya-Pinto, A.; Mao, Z.; Gobbi, M.; Yan, W.; Guo, Y.; Atxabal, A.; Llopis, R.; Yu, G.; Liu, Y.; Chuvilin, A.; Casanova, F.; Hueso, L. E. Active Morphology Control for Concomitant Long Distance Spin Transport and Photoresponse in a Single Organic Device. *Adv. Mater.* **2016**, *28*, No. 2609.
- (30) Shim, J. H.; Raman, K. V.; Park, Y. J.; Santos, T. S.; Miao, G. X.; Satpati, B.; Moodera, J. S. Large Spin Diffusion Length in an Amorphous Organic Semiconductor. *Phys. Rev. Lett.* **2008**, *100*, No. 226603.
- (31) Zhang, X.; Ma, Q.; Suzuki, K.; Sugihara, A.; Qin, G.; Miyazaki, T.; Mizukami, S. Magnetoresistance Effect in Rubrene-Based Spin Valves at Room Temperature. *ACS Appl. Mater. Interfaces* **2015**, *7*, 4685–4692.
- (32) Liang, S.; Geng, R.; Yang, B.; Zhao, W.; Subedi, R. C.; Li, X.; Han, X.; Nguyen, T. D. Curvature-enhanced Spin-orbit Coupling and Spinterface Effect in Fullerene-based Spin Valves. *Sci. Rep.* **2016**, *6*, No. 19461.
- (33) Zhang, X.; Mizukami, S.; Kubota, T.; Ma, Q.; Oogane, M.; Naganuma, H.; Ando, Y.; Miyazaki, T. Observation of a Large Spin-Dependent Transport Length in Organic Spin Valves at Room Temperature. *Nat. Commun.* **2013**, *4*, No. 1392.
- (34) Ding, S.; Tian, Y.; Wang, H.; Zhou, Z.; Mi, W.; Ni, Z.; Zou, Y.; Dong, H.; Gao, H.; Zhu, D.; Hu, W. Reliable Spin Valves of Conjugated Polymer Based on Mechanically Transferrable Top Electrodes. *ACS Nano* **2018**, *12*, 12657–12664.
- (35) Li, F.; Li, T.; Chen, F.; Zhang, F. Excellent Spin Transport in Spin Valves Based on the Conjugated Polymer with High Carrier Mobility. *Sci. Rep.* **2015**, *5*, No. 9355.
- (36) Zhang, X.; Tong, J.; Zhu, H.; Wang, Z.; Zhou, L.; Wang, S.; Miyashita, T.; Mitsuishi, M.; Qin, G. Room Temperature Magneto-resistance Effects in Ferroelectric Poly(vinylidene fluoride) Spin Valves. *J. Mater. Chem. C* **2017**, *5*, 5055–5062.
- (37) Gao, D.; Chen, Z.; Mao, Z.; Huang, J.; Zhang, W.; Li, D.; Yu, G. Highly Coplanar Bis(thiazol-2-yl)-diketopyrrolopyrrole Based Donor-Acceptor Copolymers for Ambipolar Field Effect Transistors. *RSC Adv.* **2016**, *6*, 78008–78016.
- (38) Yu, J.; Ornelas, J. L.; Tang, Y.; Uddin, M. A.; Guo, H.; Yu, S.; Wang, Y.; Woo, H. Y.; Zhang, S.; Xing, G.; Guo, X.; Huang, W. *ACS Appl. Mater. Interfaces* **2017**, *9*, 42167–42178.
- (39) Boehme, C. Organic spintronics: Window of Opportunity. *Nat. Phys.* **2017**, *13*, 928–929.
- (40) Yun, H. J.; Kang, S. J.; Xu, Y.; Kim, S. O.; Kim, Y. H.; Noh, Y. Y.; Kwon, S. K. Dramatic Inversion of Charge Polarity in Diketopyrrolopyrrole-Based Organic Field-Effect Transistors via a Simple Nitrile Group Substitution. *Adv. Mater.* **2014**, *26*, 7300–7307.
- (41) Park, K. H.; Cheon, K. H.; Lee, Y. J.; Chung, D. S.; Kwon, S. K.; Kim, Y. H. Isoindigo-Based Polymer Field-Effect Transistors: Effects of Selenophene-Substitution on High Charge Carrier Mobility. *Chem. Commun.* **2015**, *51*, 8120–8122.
- (42) Huang, J.; Mao, Z.; Chen, Z.; Gao, D.; Wei, C.; Zhang, W.; Yu, G. Diazaaisoindigo-Based Polymers with High-Performance Charge-Transport Properties: From Computational Screening to Experimental Characterization. *Chem. Mater.* **2016**, *28*, 2209–2218.
- (43) Liu, F.; Wang, H.; Zhang, Y.; Wang, X.; Zhang, S. Synthesis of Low Band-Gap 2D Conjugated Polymers and Their Application for Organic Field Effect Transistors and Solar Cells. *Org. Electron.* **2019**, *64*, 27–36.
- (44) Bredas, J.-L. Mind the Gap! *Mater. Horiz.* **2014**, *1*, 17–19.
- (45) Huang, J.; Chen, Z.; Mao, Z.; Gao, D.; Wei, C.; Lin, Z.; Li, H.; Wang, L.; Zhang, W.; Yu, G. Tuning Frontier Orbital Energetics of Azaaisoindigo-Based Polymeric Semiconductors to Enhance the Charge-Transport Properties. *Adv. Electron. Mater.* **2017**, *3*, No. 1700078.
- (46) Lin, R.; Wang, F.; Rybicki, J.; Wohlgenannt, M.; Hutchinson, K. A. Distinguishing Between Tunneling and Injection Regimes of Ferromagnet/Organic Semiconductor/Ferromagnet Junctions. *Phys. Rev. B* **2010**, *81*, No. 195214.
- (47) Santos, T. S.; Lee, J. S.; Migdal, P.; Lekshmi, I. C.; Satpati, B.; Moodera, J. S. Room-Temperature Tunnel Magnetoresistance and Spin-Polarized Tunneling through an Organic Semiconductor Barrier. *Phys. Rev. Lett.* **2007**, *98*, No. 016601.
- (48) Nguyen, T. D.; Wang, F.; Li, X.-G.; Ehrenfreund, E.; Vardeny, Z. V. Spin Diffusion in Fullerene-Based Devices: Morphology Effect. *Phys. Rev. B* **2013**, *87*, No. 075205.
- (49) Li, F. Effect of Substrate Temperature on the Spin Transport Properties in C<sub>60</sub>-Based Spin Valves. *ACS Appl. Mater. Interfaces* **2013**, *5*, 8099–8104.